

Article

A Novel Strategy for the Preparation of Supported Pd as an Efficient Catalyst for the Hydrogenation of Nitrobenzene in Mild Conditions

Zhi Hu ¹, Yiyi Cheng ¹, Meng Wu ¹, Ying Duan ^{2,3}, Yanliang Yang ^{2,*} and Tianliang Lu ^{1,*}

¹ School of Chemical Engineering, Zhengzhou University, Zhengzhou 450001, China; wmhzuuu@163.com (Z.H.); 18816706408@163.com (Y.C.); 15090331032@163.com (M.W.)

² College of Food and Drug, Luoyang Normal University, Luoyang 471934, China; duanying@mail.ustc.edu.cn

³ Henan Key Laboratory of Function-Oriented Porous Materials, College of Chemistry and Chemical Engineering, Luoyang Normal University, Luoyang 471934, China

* Correspondence: yangyli@mail.ustc.edu.cn (Y.Y.); lutianliang@zzu.edu.cn (T.L.)

Abstract: An advanced strategy was developed for the synthesis of molecular sieve-supported Pd catalysts. In this method, reductant containing C=C was in-situ prepared and pre-dispersed in the pore of the zeolites. The C=C group in the reductant can reduce the Pd²⁺ to Pd⁰ efficiently, leading to the formation of small and uniform Pd nanoparticles (~2 nm). The physical and chemical properties of the catalyst were characterized by XRD, TEM, XPS (ICP-OES), N₂ isothermal adsorption-desorption, and H₂-TPR. These catalysts showed high catalytic performance for the hydrogenation of nitrobenzene to aniline. All the TOFs for 1.5 Pd/Y, 1.5 Pd/ZSM-5, and 1.5 Pd/MOR with 1.5 wt% Pd loading are higher than 1000 h⁻¹ at 30 °C and 0.1 MPa H₂. Meanwhile, kinetic analysis for 2.0 Pd/Y was carried out, and an apparent activation energy of 28.88 kJ mol⁻¹ was obtained, which is lower than most of the reported values in the literature. Furthermore, these catalysts were stable and recyclable.

Keywords: Pd; in-situ reduction; hydrogenation; molecular sieve



Citation: Hu, Z.; Cheng, Y.; Wu, M.; Duan, Y.; Yang, Y.; Lu, T. A Novel Strategy for the Preparation of Supported Pd as an Efficient Catalyst for the Hydrogenation of Nitrobenzene in Mild Conditions. *Catalysts* **2023**, *13*, 1438. <https://doi.org/10.3390/catal13111438>

Academic Editors: Moris S. Eisen, Simona M. Coman and Werner Oberhauser

Received: 9 October 2023

Revised: 3 November 2023

Accepted: 13 November 2023

Published: 14 November 2023



Copyright: © 2023 by the authors. Licensee MDPI, Basel, Switzerland. This article is an open access article distributed under the terms and conditions of the Creative Commons Attribution (CC BY) license (<https://creativecommons.org/licenses/by/4.0/>).

1. Introduction

Heterogeneous catalysis is a commonly used strategy in many chemical processes [1,2]. Various elements, including metal [3–8] and non-metal [9], have been developed as catalytic active components. In these catalytic active elements, noble metals have attracted much attention for the catalytic hydrogenation or oxidation process due to the suitable empty d orbitals, which led to high catalytic activity, high selectivity, and mild reaction conditions [10]. In most cases, the catalytic performances of the noble metal catalysts are closely related to their particle size. A small and uniform particle size is essential for the desired performance [11]. Otherwise, high dispersion of particles can enhance the atom utilization of the noble metal, which will reduce the catalyst cost. Application of supports is efficient for the dispersion of noble metals [12,13].

Until now, various materials, including carbon [14], zeolites [15–17], metal oxide [18–20], and metal-organic frameworks [21], have been explored as supports for the synthesis of supported noble metal catalysts. In these materials, zeolites gain much attention because of their high surface area, high stability, and tunable porosity and acidity [22–24]. In the literature, many zeolites supported by noble metal catalysts were prepared by conventional impregnation [25,26] or sol-gel deposition methods [27]. In most of these catalysts, noble metals with <10 nm particle size can be easily obtained. To achieve higher dispersion of noble metals in zeolites, researchers have developed many novel synthesis strategies. For example, by introducing noble metal particles and/or clusters into the gel for zeolites synthesis, encapsulated noble metal with a 2–3 nm particle size in zeolites could be synthesized through hydrothermal methods. Furthermore, these catalysts usually show high stability.

However, most of these synthesis processes were complex and took a long time. Thus, the development of a new, easy strategy for the synthesis of zeolites supported by noble metal catalysts is necessary and meaningful.

Hydrogenation of nitrobenzene is an economical method for the production of aniline, azoxybenzene, and azobenzene [28–30], which are important intermediates in the fields of dyes, pigments, pharmaceuticals, and agricultural chemicals [31]. However, high pressure, high temperature, and/or long reaction times are generally necessary in current hydrogenation methods, leading to an increase in production costs [32]. Reactions under mild conditions would be favorable for improving industrial efficiency and environmental protection. Therefore, it is of great significance to develop a highly active catalyst for the hydrogenation of nitrobenzene. Noble metals, such as Pt [3–6] and Pd [7], usually show high catalytic activity in hydrogenation. Especially supported Pd-based catalysts have been developed for the hydrogenation of nitrobenzene. However, the development of an easy and efficient synthesis method for Pd-based catalysts to realize the hydrogenation of nitrobenzene under room temperature and normal pressure is still a challenging task.

In this work, a novel strategy was explored for the synthesis of a zeolite-supported Pd catalyst. As reported in our previous work, chemicals containing C=C groups can act as reductants for the reduction of Pd²⁺ to Pd⁰ [21]. Here, in-situ production of reductant is realized in the synthesis of the Pd-based catalyst. By this method, the reductant can be pre-dispersed uniformly in the zeolite. After the introduction of PdCl₂, the reduction of Pd²⁺ to Pd⁰ will occur uniformly on these reductant sites, leading to the formation of small and uniform Pd nanoparticles. The prepared zeolites supported by Pd catalysts were applied in the hydrogenation of nitrobenzene under room temperature and normal pressure, and a completed nitrobenzene conversion with 100% aniline selectivity was obtained. This work will provide a novel and powerful synthesis strategy for supported Pd-based catalysts.

2. Results and Discussion

2.1. Textural Properties of the Pd/Y, Pd/ZSM-5, and Pd/MOR

Zeolites have a high surface area and high stability due to their porous and crystalline structure. So the zeolites gain much attention from researchers in the field of heterogeneous catalysts. Keeping the zeolitic structure unbroken is essential for the synthesis of zeolites as catalysts. The X-ray diffraction patterns (XRD) of the prepared Pd-based catalysts and the parent zeolites are shown in Figure 1. The catalysts of 1.5 Pd/Y, 1.5 Pd/ZSM-5, and 1.5 Pd/MOR show typical FAU, MFI, and MOR topological structures, respectively. Meanwhile, compared to the XRD of parent zeolites, no obvious change was observed in the XRD patterns of 1.5 Pd/Y, 1.5 Pd/ZSM-5, and 1.5 Pd/MOR. These results mean that the synthesis processes did not destroy the crystalline structure of the zeolites [24,33–35], although NaOH was used as a catalyst for condensation reactions in the preparation of the catalysts. To study the chemical composition of the zeolites after loading Pd, the inductively coupled plasma spectrometer (ICP) method was applied to determine the $n_{(\text{Si})}/n_{(\text{Al})}$ of the samples (Table 1). It can be seen that the $n_{(\text{Si})}/n_{(\text{Al})}$ value of the sample after loading of Pd is close to that of the parent zeolite. In the synthesis process, the concentration of the NaOH solution applied as the condensation catalyst is only ~0.5 wt%; meanwhile, this process was conducted at room temperature. Thus, no significant difference in the chemical composition of the zeolites is reasonable. This is consistent with the XRD results. Meanwhile, it is reported that the characteristic diffraction peak of the Pd (111) plane should be located at $2\theta = 40.1^\circ$ [36]. However, no apparent peak corresponding to Pd (111) can be observed even in the enlarged figure. This might be caused by the small and uniform Pd particles. ICP results confirmed the presence of Pd in the catalyst. For 1.5 Pd/Y, 1.5 Pd/ZSM-5, and 1.5 Pd/MOR, the Pd loadings tested by ICP were 1.43 wt%, 1.36 wt%, and 1.39 wt%, respectively (Table 1). Based on the theoretical value (1.5 wt%), it can be concluded that more than 90% of the Pd was successfully introduced into these zeolitic catalysts. Thus, the absence of a diffraction peak of Pd in XRD results implies the presence of small and uniform Pd particles in the catalysts. Otherwise, surface area and pore volume

were measured and listed in Table 1. All the prepared Pd-containing catalysts show high surface area and pore volume, and this is caused by the porous structure of the zeolites. Compared with supports (Y, ZSM-5, MOR), prepared catalysts (1.5 Pd/Y, 1.5 Pd/ZSM-5, and 1.5 Pd/MOR) have a lower surface area and pore volume, implying the successful loading of Pd, which can block some pores in the zeolite.

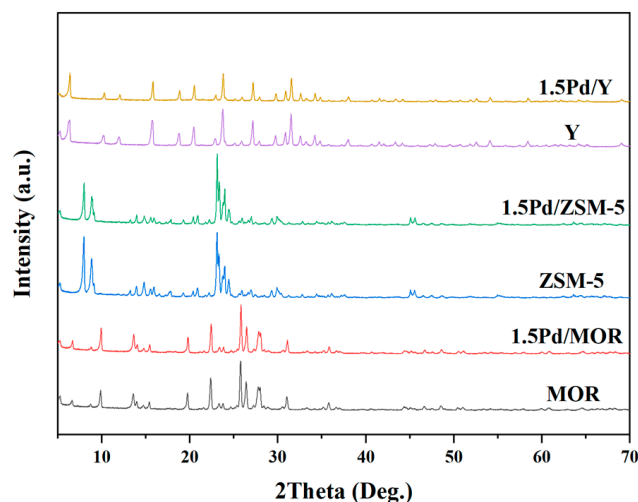


Figure 1. XRD pattern of a Pd-based catalyst supported by a molecular sieve with 1.5 wt% loading.

Table 1. Textural parameters of the samples.

Samples	BET Surface Area ($\text{m}^2 \text{g}^{-1}$)	Pore Volume ($\text{cm}^3 \text{g}^{-1}$)	Pd Content (wt%)	$n_{\text{(Si)}}/n_{\text{(Al)}}$
Y	623	0.33	-	13.8
1.5 Pd/Y	566	0.30	1.43	13.1
ZSM-5	390	0.22	-	28.3
1.5 Pd/ZSM-5	289	0.20	1.36	27.9
MOR	457	0.20	-	13.0
1.5 Pd/MOR	453	0.19	1.39	12.5

The target of the developed synthesis method of the Pd-based catalyst in this work is to get small and uniform Pd nanoparticles showing good catalytic performances in hydrogenation. To get information about Pd particles directly, transmission electron microscope (TEM) images of the prepared catalysts were collected. As shown in Figure 2, many small black spots can be observed on the supports in the images for 1.5 Pd/Y, 1.5 Pd/MOR, and 1.5 Pd/ZSM-5. These black spots confirmed the presence of Pd particles in the catalysts. Particle sizes of the Pd were measured and shown in Figure 2. For 1.5 Pd/Y, 1.5 Pd/MOR, and 1.5 Pd/ZSM-5, the Pd particle sizes are ~ 1.66 , ~ 2.41 , and ~ 1.64 nm, respectively, illustrating the small and uniform Pd particle size in these catalysts. This is consistent with the absence of a diffraction peak for Pd in the XRD results. Overall, the Pd particle sizes for these samples are around 2 nm. And the difference in these metal particle sizes is not obvious. These results indicate that the synthesis method developed in this work is efficient for the preparation of zeolites supported by Pd catalysts with small and uniform Pd nanoparticles.

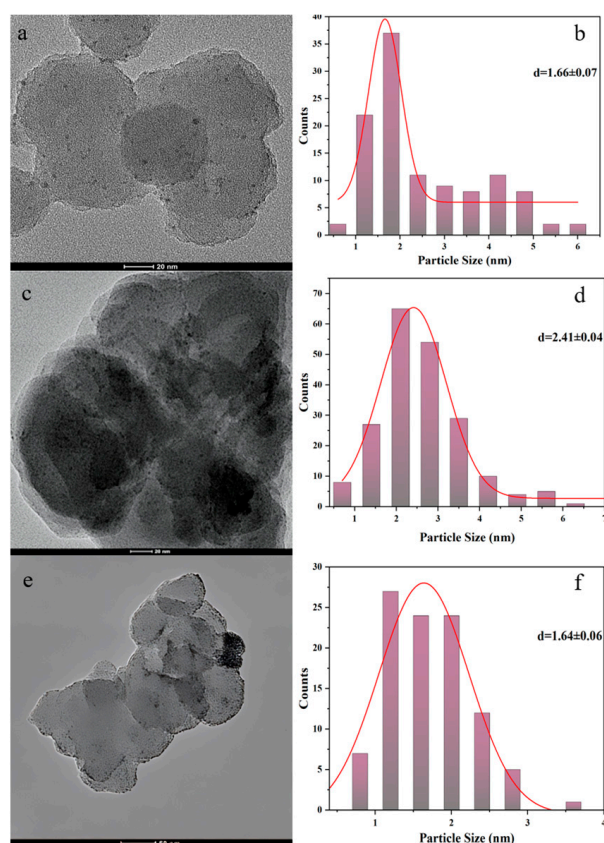


Figure 2. TEM images and particle size distributions of 1.5 Pd/Y (a,b), 1.5 Pd/MOR (c,d), and 1.5 Pd/ZSM-5 (e,f).

In this work, a new synthesis method for a Pd-based catalyst was developed where condensation products of 1,3,5-triformylbenzene and ketone were used as in situ reductants for the reduction of Pd^{2+} to Pd^0 . The reduction efficiency of the in-situ-prepared reductants is important for this synthesis strategy. To determine the chemical state of the Pd in the prepared catalyst, X-ray photoelectron spectroscopy (XPS) of 1.5 Pd/Y was collected. As shown in Figure 3a, elements of Na, O, Si, and Al were detected in the composition of Y zeolite. Meanwhile, Pd was also detected, illustrating the successful loading of Pd into zeolite. Figure 3b shows the XPS spectrum of Pd 3d. Two strong peaks located at 335.5 and 340.8 eV are observed, which can be ascribed to Pd^0 3d_{5/2} and Pd^0 3d_{3/2}, respectively [37]. Meanwhile, two weak peaks located at 336.8 and 342.0 eV are also detected, which can be assigned to Pd^{2+} 3d_{5/2} and Pd^{2+} 3d_{3/2}, respectively [36]. These results imply that most of the Pd in the catalyst is in Pd^0 form, which provides the active sites for hydrogenation. Besides Pd^0 , a small amount of Pd^{2+} was also detected in the catalyst. This is a common phenomenon for Pd-based catalysts in the literature [38]. Some surface Pd^0 species can be oxidized to Pd^{2+} in the air, which can be easily detected by XPS, a surface-sensitive characterization method.

As expected, the condensation product of 1,3,5-triformylbenzene and acetone containing C=C bonds can realize the reduction of Pd^{2+} to Pd^0 efficiently. Thus, the reduction method developed in this work provides an in-situ reductant production strategy for the synthesis of Pd-based catalysts.

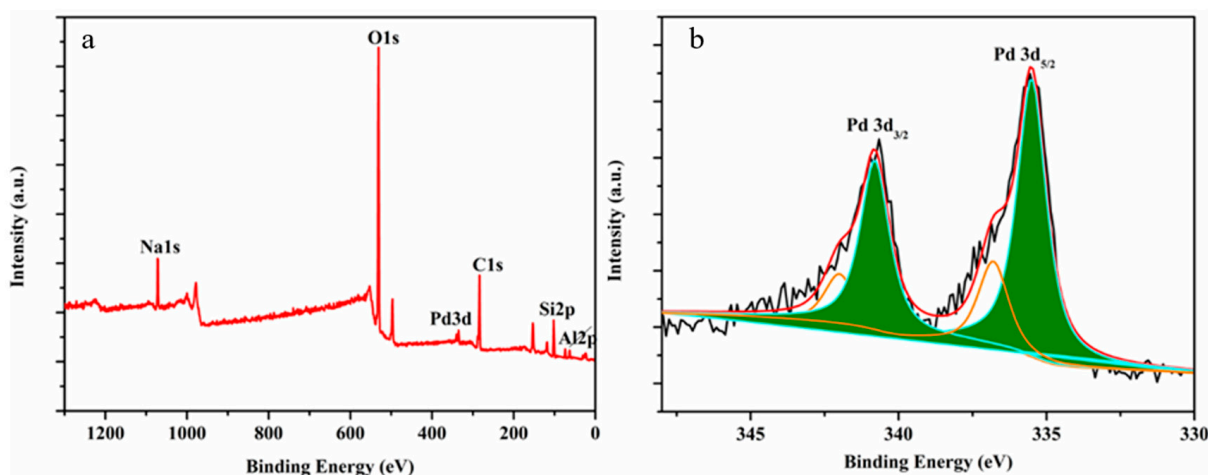
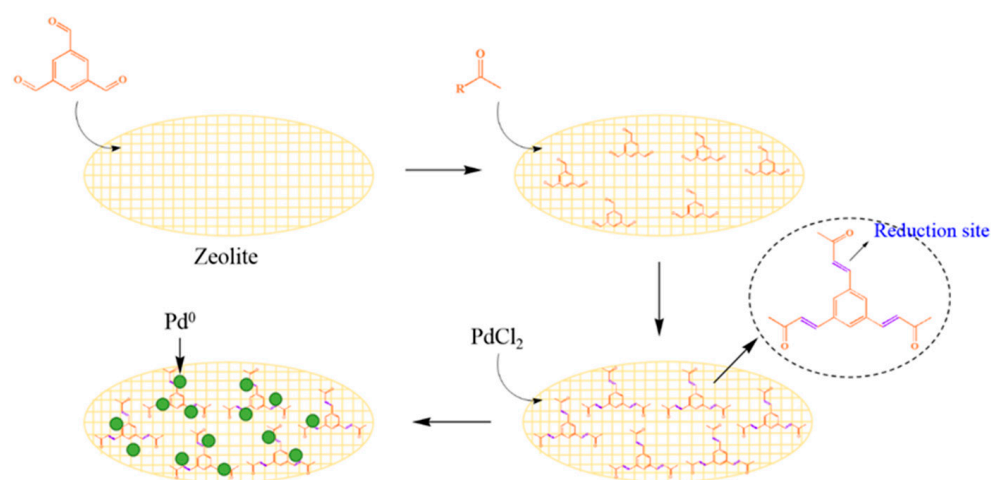


Figure 3. (a) The full-range XPS spectra of 1.5 Pd/Y; (b) Pd 3D spectra of 1.5 Pd/Y.

As reported in our previous work, the C=C group can realize the reduction of Pd²⁺ to Pd⁰ through the Wacker reaction [39,40]. When palladium chloride reacted with cyclohexene in an aqueous solution, palladium black was obtained, and the generation of cyclohexanone was detected [40]. By using a base as a catalyst, chemicals with C=C groups can be synthesized by aldol condensation. Thus, in this work, a reducing agent containing C=C groups was in-situ synthesized by aldol condensation between 1,3,5-triformylbenzene and ketone (such as acetone) in the preparation of the catalyst. Based on the characterization results discussed above, the synthesis scheme for zeolites supported by Pd is proposed (Scheme 1). Firstly, 1,3,5-triformylbenzene was introduced into the zeolite uniformly by an impregnation method. Then, ketone solutions and bases (such as NaOH) were added. The base acts as the catalyst in the aldol condensation reaction between 1,3,5-triformylbenzene and ketone. After reacting for a desired time, the aldol condensation product with C=C groups formed uniformly in the zeolite. The C=C group in the condensation product has reduction ability. When PdCl₂ is loaded, the Pd²⁺ can be reduced to Pd⁰ on these C=C sites in the presence of water through a partial Wacker reaction. The uniform dispersion of the in-situ-formed reducing agent on zeolite can ensure the formation of small and uniform Pd⁰ nanoparticles, which provide highly active sites for various hydrogenation reactions. This is a novel, easy, and efficient strategy for the synthesis of zeolites supported by Pd catalysts. This method can also be applied to the synthesis of other supported noble metal catalysts.



Scheme 1. The proposed synthesis scheme for zeolite-supported Pd was developed in this work.

2.2. Catalytic Tests

Generally, supported Pd-based catalysts with small and uniform Pd⁰ nanoparticles show high catalytic activity in various reactions such as hydrogenation and oxidation. Zeolites supported by Pd synthesized in this work have satisfied Pd⁰ dispersion (about 2 nm). The catalytic performance of these catalysts is anticipated. The catalytic performances of 1.5 Pd/Y, 1.5 Pd/ZSM-5, and 1.5 Pd/MOR on hydrogenation of nitrobenzene were tested, and the results are shown in Figure 4. For comparison, blank reactions with no catalyst and with the catalyst of parent Y zeolite were conducted. The tests were carried out at room temperature (30 °C) and an atmospheric pressure of H₂ (0.1 MPa). As anticipated, no product was detected for the blank reactions after reaction for 1 h. For 1.5 Pd/Y, 1.5 Pd/ZSM-5, and 1.5 Pd/MOR, high nitrobenzene conversion (>70%) and aniline selectivity (>95%) were observed under the same conditions. In particular, 98% nitrobenzene conversion with 100% aniline selectivity was obtained for 1.5 Pd/MOR. The 1.5 Pd/MOR with a particle size of 2.41 nm has the highest catalytic activity of these three catalysts. The slight differences in particles (~1.66, ~2.41, and ~1.64 nm) may not be the main reason for their different catalytic activity. TOF values for the catalysts are calculated based on the results of the catalytic tests. As shown in Figure 4, TOFs for 1.5 Pd/Y, 1.5 Pd/ZSM-5, and 1.5 Pd/MOR are 1094, 1365, and 1548 h⁻¹, respectively. These values are higher than those of other catalysts for the reduction of nitrobenzene. As listed in Table 2, the TOF of the non-noble metal catalyst Ni/C is only 1 h⁻¹, which is much lower than that of the Pd and Ag-based catalysts. Pd-based catalysts are the most studied for the reduction of nitrobenzene. However, these Pd-based catalysts reported in the literature show great catalytic activity differences. For Pd/ox-CEINs and Pd@CTF, TOFs are 103 and 495 h⁻¹, respectively. In our previous work, the TOF value for a Pd-based catalyst in the reduction of nitrobenzene was enhanced to 984 h⁻¹ by using Pd/CTF as a catalyst. Satisfactorily, in this work, much higher TOF values were obtained. An outstanding TOF value of 1548 h⁻¹ for 1.5 Pd/MOR will give a deep impression to the researchers. These TOF values are much higher than those in the literature, indicating the advantage of the method developed in this work for the synthesis of molecular sieve-supported Pd catalysts with high catalytic activity. Otherwise, the mild reaction conditions applied in this work are competitive and attractive as to energy conservation and operation safety. High conversion (close to complete conversion) couldn't efficiently reflect the effects of factors including ketone structure and Pd loading on the catalytic performances in the following study. A moderate conversion is proper. However, making the conversion lower by changing the reaction conditions is difficult because the reaction conditions in this work are so mild. In 1.5 Pd/Y, 1.5 Pd/ZSM-5, and 1.5 Pd/MOR, 1.5 Pd/Y shows a moderate nitrobenzene conversion, which is convenient for further studying the catalytic performances. In the following study, 1.5 Pd/Y was selected as the catalyst for the hydrogenation of nitrobenzene.

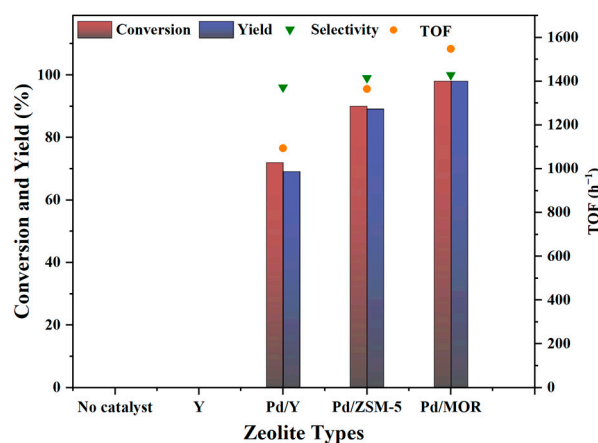


Figure 4. Effect of zeolite types on the hydrogenation performance of catalysts.

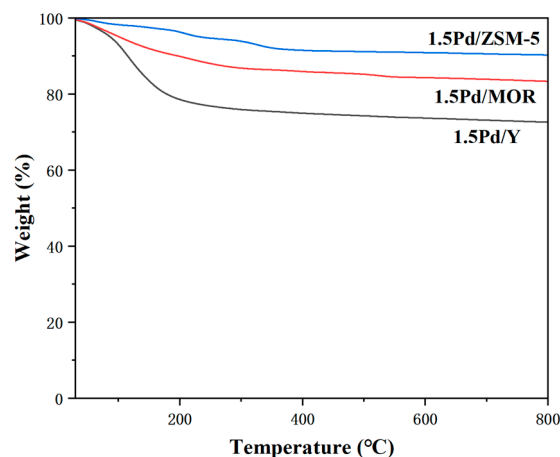
Table 2. Catalytic activity of different catalysts in the reduction of nitrobenzene.

Entry	Catalyst	Temperature (°C)	Time (h)	TOF ^b (h ⁻¹)	References
1	Ni/C	40	4	1	[41]
2	Pd/ox-CEINs ^a	70	1	103	[42]
3	Ag/ α -Fe ₂ O ₃	100	0.5	248	[43]
4	Pd@CTF ^a	25	0.2	495	[44]
5	Pd/CTF ^a	30	0.5	984	[21]
6	1.5 Pd/Y	30	1	1094	This work
7	1.5 Pd/ZSM-5	30	1	1365	This work
8	1.5 Pd/MOR	30	1	1548	This work

^a ox-CEINs, oxidized carbon-encapsulated iron nanoparticles; CTF covalent-triazine framework. ^b TOF was calculated based on the total Pd content in the catalyst.

Reaction condition: 0.64 mmol of nitrobenzene, 3.0 mg of catalyst, 0.1 MPa H₂, 30 °C, 1 h, 1200 rpm.

TG results can give some information about the organic residue in the catalysts. As shown in Figure 5, for all these catalysts, the weight loss mainly occurred in the temperature range of 50–200 °C. The weight loss in this region was caused by the removal of water, and some organic residues were not removed by washing in the synthesis of the Pd-based catalysts. Obvious weight losses were observed in the TG curves of Pd/ZSM-5, Pd/MOR, and Pd/Y, indicating the existence of some organic residue in the prepared catalyst. These residues were adsorbed into the structure of the zeolites. The washing process cannot remove it completely. Meanwhile, the adsorption strengths of the residues in the three zeolites are different, leading to a different weight loss ratio. This might be related to the differences in the microenvironment of these zeolites. Fortunately, these prepared catalysts still show high catalytic performance, although some residue exists in the catalyst. This encourages us to do more work to remove the residue to further enhance the catalytic performance of these catalysts in the future.

**Figure 5.** TG curves of 1.5 Pd/ZSM-5, 1.5 Pd/MOR, and 1.5 Pd/Y.

Considering Pd nanoparticles are the active sites in the hydrogenation of nitrobenzene, the effect of Pd loading was investigated. As shown in Figure 6, with an increase in Pd loading from 0.5 wt% to 1.5 wt%, the conversion of nitrobenzene increases greatly from 26% to 72%. When the Pd loading is increased to 2.0 wt%, 100% nitrobenzene conversion is obtained. Meanwhile, the selectivity of aniline also increases with an increase in Pd loading. Particularly, 100% nitrobenzene conversion with 100% aniline selectivity was obtained for 2.0 Pd/Y. For 2.5 Pd/Y, similar catalytic performances with 2.0 Pd/Y are observed under the same reaction conditions. In order to better understand the catalytic behavior of palladium, H₂-TPR was conducted. As shown in Figure 7, the reduction peaks at ~280, ~360, and ~510 °C are observed. As reported in the literature [45–47], Pd²⁺ is easily reduced

to Pd⁰ at low temperatures (<100 °C). The reduction peak at higher temperatures can be ascribed to the reduction of highly dispersed and/or encapsulated Pd species, which react strongly with the zeolitic support. In this work, most of the Pd was in Pd⁰ form, and the rest was in Pd²⁺ form, as illustrated by the XPS result. In 0.5 Pd/Y, there was only one weak peak at ~510 °C, which was caused by the reduction of Pd²⁺, which might be in the framework of the zeolite having the strongest interaction with the zeolite. For 1.5 Pd/Y, 2.0 Pd/Y, and 2.5 Pd/Y, two peaks at ~360 and ~280 °C might be attributed to the reduction of Pd²⁺ species inside and outside the zeolite having moderate interaction with the support. Overall, with the increase in Pd loading, the intensity of the reduction peak for Pd²⁺ outside the zeolite increases. This can be explained by the fact that the amount of reductant formed by in-situ condensation in zeolite is unchanged in the synthesis process. Higher Pd loading means a lower reductant/PdCl₂ ratio, which leads to more unreduced Pd²⁺ species. For 0.5 Pd/Y and 1.5 Pd/Y, all the reduction peaks are very weak, implying excessive reducibility of the in-situ-formed reductant in support of the synthesis of these catalysts. For 2.0 Pd/Y, the amount of unreduced Pd²⁺ increases, obviously indicating the depleted reducibility of the reductant in support. Thus, with the increase in Pd loading from 0.5% to 2%, the amount of Pd⁰ in the prepared catalyst increases, leading to higher catalytic activity. Considering the catalytic performance, 2.0 Pd/Y was selected as the catalyst in the following study.

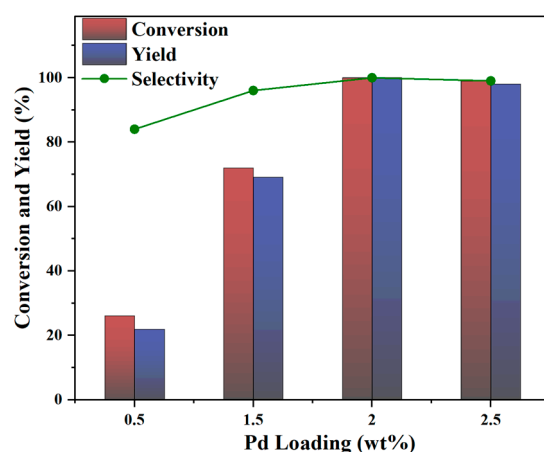


Figure 6. Effect of palladium loading on the hydrogenation performance of catalysts.

Reaction condition: 0.64 mmol of nitrobenzene, 3.0 mg of catalyst, 0.1 MPa H₂, 30 °C, 1 h, 1200 rpm.

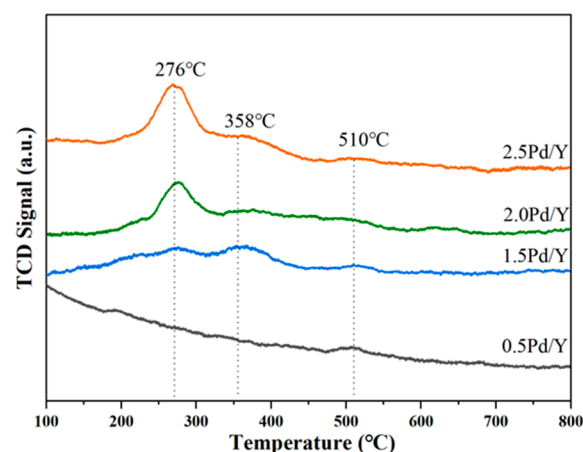


Figure 7. H₂-TPR profile of the Pd/Y catalysts.

As mentioned above, ketones were applied for the in-situ synthesis of reductant, which is essential for the reduction of PdCl_2 to Pd^0 . Ketones, including acetone, butanone, cyclopentanone, and cyclohexanone, were used to study the effect of ketone types on the catalytic performance of the catalyst. As shown in Figure 8, when acetone and butanone were applied to synthesize the reductant, the prepared catalyst showed high catalytic activity ($\sim 100\%$ nitrobenzene conversion). However, lower catalytic activities were observed when cyclopentanone and cyclohexanone were used. This is related to the molecular structure of the ketones. Acetone and butanone have chain-type molecular structures, while cyclopentanone and cyclohexanone have cyclic structures. For the introduction of reductant into the zeolite, condensation products derived from chain-type ketones have a smaller steric hindrance than those from cyclic ketones. Thus, the reductant based on chain-type ketones can realize the reduction of Pd^{2+} to Pd^0 in zeolite more efficiently than that based on cyclic ketones, leading to the higher catalytic activity of the catalyst synthesized with the former reductants. Otherwise, the types of ketones do not influence the product selectivity. All the synthesized catalysts based on different ketones show $\sim 100\%$ aniline selectivity.

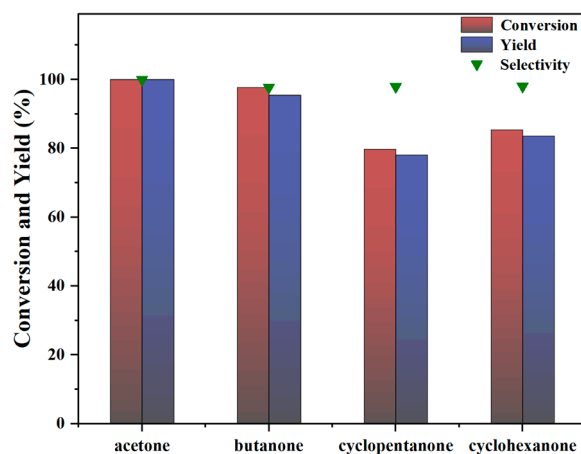


Figure 8. Effect of ketones on hydrogenation performance of catalysts.

Stability and recyclability are important for the industrial application of heterogeneous catalysts. Thus, the stability and recyclability of the prepared catalyst were tested. The results are shown in Figure 9. To reveal the real stability of the catalyst, the complete conversion of the reactant should be avoided. Thus, a reaction time of 35 min was selected. In the test, the catalyst separated from the reaction solution was directly used in the next run after drying. Slight decreases in conversion and selectivity were observed after each run. The XRD patterns of the fresh catalyst and the catalyst after the fifth run are shown in Figure 10. After several runs, the intensity of the XRD peaks became lower. This might be caused by the basicity of the product of aniline. It can damage the crystalline structure of the zeolite to some degree. Otherwise, the 2.0 Pd/Y catalyst kept the crystalline structure of the Y zeolite after 5 runs, indicating the acceptable stability of the catalyst. These results imply that the zeolite-supported Pd catalyst synthesized by the novel strategy developed in this work has industrial application potential.

To confirm the reproducibility of the catalytic performance, a scale-up reaction was tested. In this test, 6.4 mmol of nitrobenzene dissolved in ethanol (5 wt% of nitrobenzene in ethanol) and 30 mg of 2.0 Pd/Y were applied. After reaction at 30 °C for 1 h under 0.1 MPa H_2 , 98% nitrobenzene conversion with 99% aniline selectivity was obtained. This result indicates that the high catalytic performance of the prepared catalyst can be maintained in the scale-up of the reaction to some degree.

Reaction condition: 0.64 mmol of nitrobenzene, 3.0 mg of 2.0 Pd/Y, 0.1 MPa H_2 , 30 °C, 1 h, 1200 rpm.

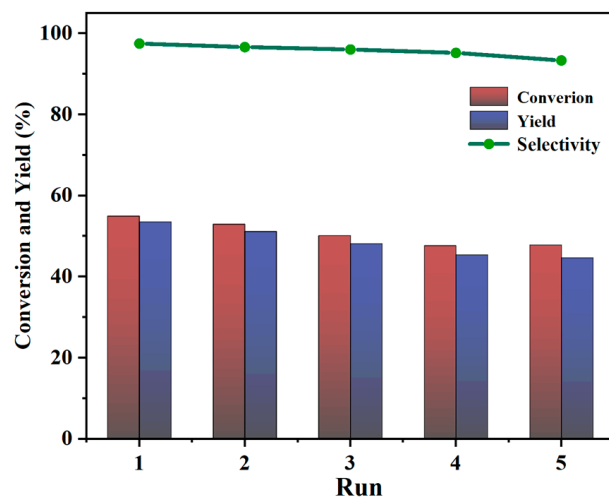


Figure 9. The catalyst recycling performance experiments.

Reaction condition: 0.64 mmol of nitrobenzene, 3.0 mg of 2.0 Pd/Y, 0.1 MPa H₂, 30 °C, 35 min, 1200 rpm.

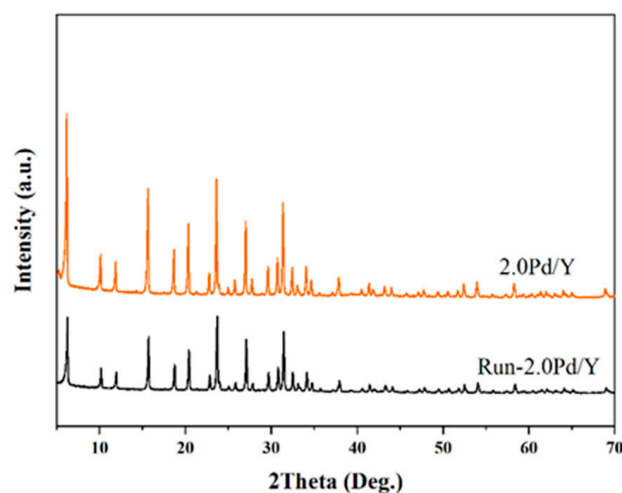


Figure 10. XRD of the fresh 2.0 Pd/Y and the used 2.0 Pd/Y after 5 runs.

The kinetic study can provide some basic parameters for the design of a reactor on an industrial scale-up. In this work, kinetic analysis was conducted by collecting the time course of the reaction at 30, 40, 50, and 60 °C. The initial concentration of nitrobenzene and the concentration of nitrobenzene at a definite reaction time were denoted as c_0 and c_a , respectively. As shown in Figure 11a–d, the linear relationship between $\ln(c_a/c_0)$ and reaction time indicates that this is a first-order reaction. Figure 11e shows the Arrhenius plot for the hydrogenation of nitrobenzene over 2.0 Pa/Y. The apparent activation energy (E_a) calculated by a linear fitting method is 28.88 kJ mol⁻¹, which is lower than most of the reported values in the literature [48], implying the higher catalytic activity of the catalyst developed in this work. Meanwhile, according to the line intercept in Figure 11e, the pre-exponential factor (A) was determined to be 29.64 s⁻¹. Thus, the Arrhenius equation for hydrogenation of nitrobenzene over 2.0 Pd/Y can be expressed as: $k = 29.64 \exp(-3473.79/T)$.

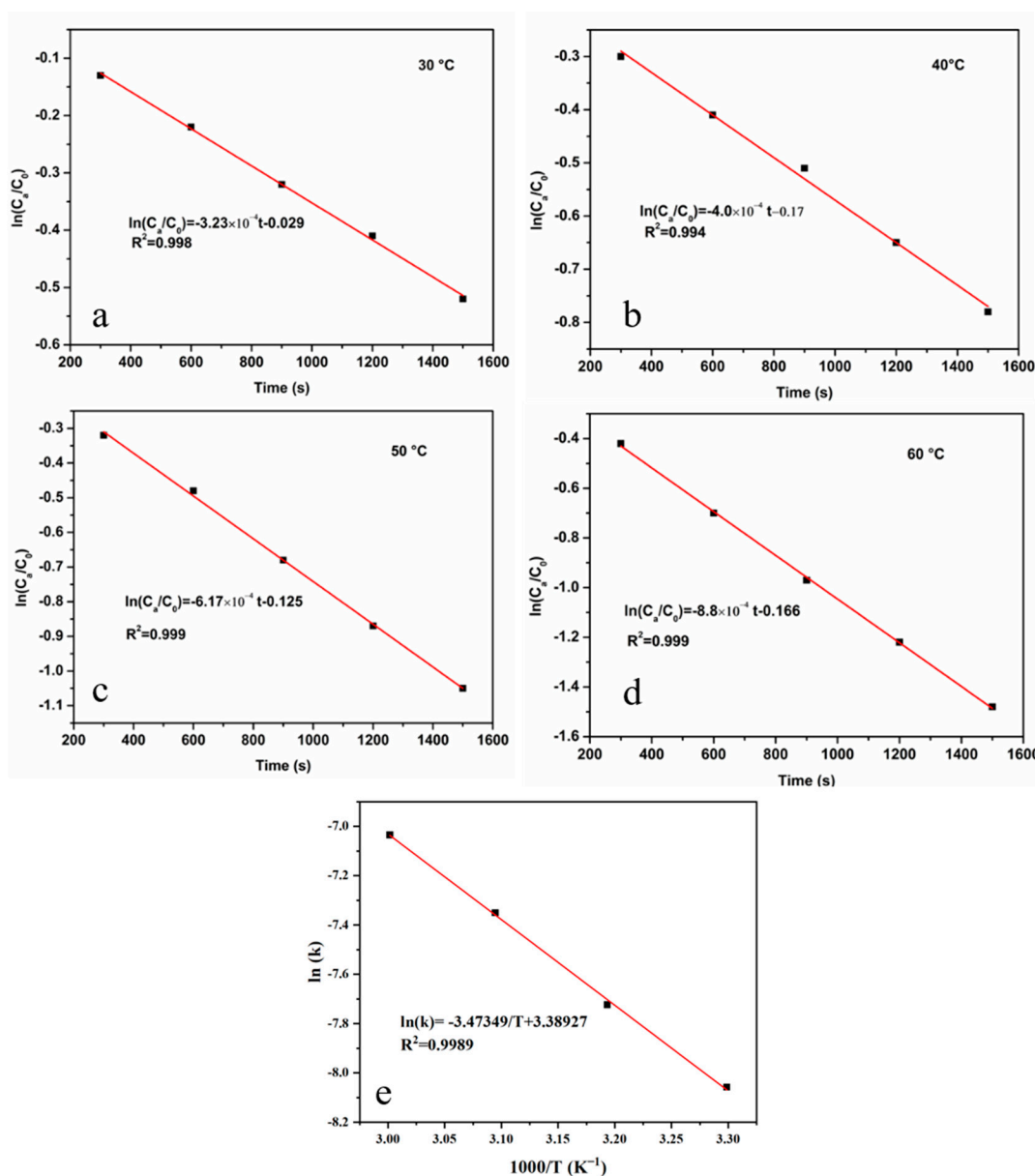


Figure 11. First-order reaction rate constants (a–d) and Arrhenius curve (e) for hydrogenation of nitrobenzene catalyzed over 2.0 Pd/Y.

Reaction condition: 0.64 mmol of nitrobenzene (5 wt% of nitrobenzene in ethanol), 3.0 mg of catalyst, 0.1 MPa H_2 , 1200 rpm.

3. Materials and Methods

3.1. Materials

Y ($n_{Si}/n_{Al} = 13.8$), MOR ($n_{Si}/n_{Al} = 13.0$), and ZSM-5 ($n_{Si}/n_{Al} = 28.3$) zeolites were purchased from Nankai University Catalyst Co., Ltd. (Tianjin, China). Before use, these zeolites were calcined at 550 °C for 6 h in air. Nitrobenzene (NB), ethanol, acetone, butanone, cyclohexanone, cyclopentanone, sodium hydroxide, palladium (II) chloride ($PdCl_2$), and cyclohexene were purchased from Aladdin Chemicals Co., Ltd. (Shanghai, China). 1,3,5-Triformylbenzene was purchased from Anneji Chemical Co., Ltd. (Shanghai, China). All other reagents were commercially available and were used as received.

3.2. Synthesis of Catalysts

A novel synthesis method was developed for the synthesis of Pd-based catalysts with small and uniform Pd⁰ nanoparticles. Details about the synthesis processes are described as follows: In a round-bottom flask, 10 mg of 1,3,5-triformylbenzene was dissolved in 5 mL of ethanol. Then, 1 g of molecular sieve (Y, MOR, or ZSM-5) was added to the solution. After stirring for 1 h at room temperature, the ethanol in the mixture was removed by rotary evaporation at 60 °C. The obtained solid was dispersed in 20 mL of deionized water, and the mixture was stirred for 0.5 h. Then, 5 mL of water solution containing 21 mg of acetone (equivalent molar ketone was calculated when another ketone was used) and 120 mg of NaOH were added drop-by-drop. After stirring for 4 h, the mixture was washed with H₂O to a neutral pH, and the desired amount of PdCl₂ aqueous (0.5 wt% of Pd²⁺ in water) was added. Finally, the solid was separated by centrifugation, washed with H₂O and ethanol several times, and dried at 60 °C overnight. The obtained catalysts were labeled as xPd/zeolite, where x represents the mass percentage of Pd.

3.3. Catalyst Characterization

X-ray diffraction (XRD) was used to characterize the crystal structure of the catalysts by using a Rigaku D/Max 2500/PC powder diffractometer with Cu K α radiation ($\lambda = 0.15418$ nm) at a scanning rate of 5° min⁻¹. The tube voltage and tube current are 40 kV and 40 mA, respectively. To get information about the particle size distribution of Pd, transmission electron microscopy (TEM) was conducted on a FEI Tecnai G2 F20 microscope at 200 kV. The Pd content of the catalyst was determined by inductively coupled plasma optical emission spectroscopy (ICP-OES) on a Thermo iCAP 6000 Series. Nitrogen adsorption and desorption were conducted on a Micrometrics ASAP 2460 adsorbent at -196 °C to get the specific surface areas and pore volumes of the catalysts. Before measurement, all the samples were pretreated at 200 °C for 3 h. The specific surface area and pore volume were calculated by the Brunauer-Emmett-Teller (BET) and *t*-plot methods, respectively. The chemical states of Pd were determined by X-ray photoelectron spectroscopy (XPS) using a Thermo ESCALAB 250Xi spectrometer equipped with Mg-K α (1253.6 eV) radiation. C 1s (284.6 eV) was used as the reference for calibration. Hydrogen temperature-programmed reduction (H₂-TPR) was carried out on a Micromeritics AutoChem II 2920 instrument. Firstly, 15 mg of the sample was heated to 200 °C at a rate of 10 °C min⁻¹ under an Ar atmosphere. After 40 min, the temperature of the sample was cooled down to 40 °C, and then the Ar was replaced by 10% Ar-H₂ mixed gas. Fifteen min later, the sample was heated to 800 °C at a rate of 10 °C min⁻¹. The hydrogen consumption was recorded by a TCD detector. Thermo Gravimetric Analyzer (TGA) The thermal stability of the catalyst was characterized by a simultaneous thermal analyzer (DTG-60H) produced by Shimadzu Corporation, Kyoto, Japan. Taking 5–10 mg of the sample and placing it in an alumina crucible and recording the signal of the sample from room temperature to 1200 °C at a heating rate of 10 °C·min⁻¹ under an air atmosphere.

3.4. Hydrogenation of Nitrobenzene

Hydrogenation of nitrobenzene was carried out in a 15-mL stainless steel autoclave with lining, a controllable pressure gauge, and magnetic stirring at room temperature under 0.1 MPa H₂. Typically, 2 mg of catalyst and 2 mL of a nitrobenzene-ethanol solution (the mass percentage of nitrobenzene is 5 wt%) were added to a reactor. After replacing the air in the reactor with H₂ four times, the H₂ pressure in the reactor was set at 0.1 MPa. Then, the reactor was sealed and stirred at 1200 rpm for 1 h. The reaction solution was analyzed by an Agilent 8860 GC with a HP-5 column and a flame ionization detector. To calculate the conversion of nitrobenzene (NB) and the selectivity of aniline (AN), naphthalene was

applied as the internal standard. The conversion of nitrobenzene and the selectivity of aniline were calculated based on the following equations:

$$\text{Conversion} = \left(1 - \frac{\text{moles of NB}}{\text{moles of nitrobenzene loaded initially}} \right) \times 100\%$$

$$\text{Selectivity} = \frac{\text{moles of AN}}{\text{moles of nitrobenzene converted}} \times 100\%$$

4. Conclusions

In conclusion, a novel, easy, and efficient synthesis strategy was developed for the preparation of supported Pd catalysts in this work. In this method, the condensation product of 1,3,5-triformylbenzene and ketone containing the C=C group was developed as a reductant of Pd²⁺ for the first time. This condensation product could be in-situ prepared and pre-dispersed in the pore of zeolites and then act as the reduction site for Pd²⁺ to Pd⁰. Using this method, zeolites supported by small and uniform Pd nanoparticles (~2 nm) can be easily obtained, showing high catalytic hydrogenation activity. As to hydrogenation of nitrobenzene to aniline, all the TOFs for 1.5 Pd/Y, 1.5 Pd/ZSM-5, and 1.5 Pd/MOR with 1.5 wt% Pd loading are higher than 1000 h⁻¹ at 30 °C and 0.1 MPa H₂; meanwhile, complete conversion with 100% aniline selectivity can be obtained. Otherwise, apparent activation energy was calculated as 28.88 kJ mol⁻¹ based on kinetic analysis for 2.0 Pd/Y. This is lower than most of the reported values in the literature. Furthermore, recycling tests indicate the prepared catalyst is recyclable. This work provides an attractive synthesis method for zeolites supported by Pd catalysts. In the future, this method can be modified and applied to the synthesis of other supported noble metal catalysts.

Author Contributions: Conceptualization, T.L. and Y.Y.; methodology, Z.H.; validation, Y.C. and M.W.; investigation, M.W.; data curation, Y.C.; writing—original draft preparation, Z.H.; writing—review and editing, T.L.; visualization, Y.Y.; supervision, T.L.; project administration, T.L. and Y.D.; funding acquisition, T.L. and Y.D. All authors have read and agreed to the published version of the manuscript.

Funding: This research was funded by the Education Department of Henan Province (2021GGJS133) and the China Postdoctoral Science Foundation (2023M733216).

Data Availability Statement: No additional data are available.

Conflicts of Interest: The authors declare no conflict of interest.

References

1. Sheldon, R.A. Recent advances in green catalytic oxidations of alcohols in aqueous media. *Catal. Today* **2015**, *247*, 4–13. [[CrossRef](#)]
2. Christoffel, F.; Ward, T.R. Palladium-Catalyzed Heck Cross-Coupling Reactions in Water: A Comprehensive Review. *Catal. Lett.* **2017**, *148*, 489–511. [[CrossRef](#)]
3. Yao, P.; Huang, Y.; Jiao, Y.; Xu, H.; Wang, J.; Chen, Y. Soot oxidation over Pt-loaded CeO₂-ZrO₂ catalysts under gasoline exhaust conditions: Soot-catalyst contact efficiency and Pt chemical state. *Fuel* **2023**, *334*, 126782.
4. Chen, Z.; Luo, D.; Zhang, H.; Zhang, N.; Li, J.; Gao, B.; Qiu, R.; Li, Y.; Yang, Z. Reaction pathway of nitric oxide oxidation on nano-sized Pt/SiO₂ catalysts for diesel exhaust purification. *Mol. Catal.* **2021**, *516*, 111991. [[CrossRef](#)]
5. Tan, W.; Xie, S.; Wang, X.; Wang, C.; Li, Y.; Shaw, T.E.; Ma, L.; Ehrlich, S.N.; Liu, A.; Ji, J.; et al. Highly efficient Pt catalyst on newly designed CeO₂-ZrO₂-Al₂O₃ support for catalytic removal of pollutants from vehicle exhaust. *Chem. Eng. J.* **2021**, *426*, 131855. [[CrossRef](#)]
6. Zhao, B.; Chen, W.; Tan, Y.; Li, F.; Tian, M. Preparation of M/Ce_{1-x}Ti_xO₂ (M=Pt, Rh, Ru) from sol-gel method and their catalytic oxidation activity for diesel soot. *J. Rare Earths* **2022**, *40*, 1849–1859. [[CrossRef](#)]
7. Zhang, S.; Feng, X.; Rao, C.; Xu, X.; Xu, J.; Fang, X.; Li, Y.; Wang, X. Engineering low Pd content catalysts for soot combustion through tuning the Pd-SnO₂ interface interaction: Disclosing the critical role of dual Pd valence states for the activity. *Appl. Catal. A Gen.* **2022**, *647*, 118906. [[CrossRef](#)]
8. Lee, J.H.; Kim, M.J.; Lee, E.J.; Lee, D.W.; Kim, C.H.; Lee, K.Y. Promoting effect of Rh-impregnation on Ag/CeO₂ catalyst for soot oxidation. *Appl. Surf. Sci.* **2022**, *572*, 151504. [[CrossRef](#)]

9. Hu, C.G.; Dai, L.M. Multifunctional Carbon-Based Metal-Free Electrocatalysts for Simultaneous Oxygen Reduction, Oxygen Evolution, and Hydrogen Evolution. *Adv. Mater.* **2017**, *29*, 1604942. [[CrossRef](#)]
10. Motokura, K.; Ding, S.; Usui, K.; Kong, Y. Enhanced Catalysis Based on the Surface Environment of the Silica-Supported Metal Complex. *ACS Catal.* **2021**, *11*, 11985–12018. [[CrossRef](#)]
11. Morawski, A.W.; Gano, M.; Ćmielewska, K.; Kusiak-Nejman, E.; Pelech, I.; Staciwa, P.; Ekiert, E.; Narkiewicz, U. Photocatalytic Reduction Efficiency of CO₂ Depending on ZnO Particle Size. *Catalysts* **2023**, *13*, 1270. [[CrossRef](#)]
12. Ma, M.; Yang, R.; He, C.; Jiang, Z.; Shi, J.W.; Albilali, R.; Fayaz, K.; Liu, B. Pd-based catalysts promoted by hierarchical porous Al₂O₃ and ZnO microsphere supports/coatings for ethyl acetate highly active and stable destruction. *J. Hazard. Mater.* **2021**, *401*, 123281. [[CrossRef](#)] [[PubMed](#)]
13. Wang, Y.; Zhang, C.; Liu, F.; He, H. Well-dispersed palladium supported on ordered mesoporous Co₃O₄ for catalytic oxidation of o-xylene. *Appl. Catal. B Environ.* **2013**, *142*, 72–79. [[CrossRef](#)]
14. Faroppa, M.L.; Chiosso, M.E.; Musci, J.J.; Ocsachoque, M.A.; Merlo, A.B.; Casella, M.L. Oxidation of Glycerol in Base-Free Aqueous Solution Using Carbon-Supported Pt and PtSn Catalyst. *Catalysts* **2023**, *13*, 1071. [[CrossRef](#)]
15. Chen, C.; Chen, F.; Zhang, L.; Pan, S.; Bian, C.; Zheng, X.; Meng, X.; Xiao, F.S. Importance of platinum particle size for complete oxidation of toluene over Pt/ZSM-5 catalysts. *Chem. Commun.* **2015**, *51*, 5936–5938. [[CrossRef](#)] [[PubMed](#)]
16. Yang, L.; Liu, Q.; Han, R.; Fu, K.; Su, Y.; Zheng, Y.; Wu, X.; Song, C.; Ji, N.; Lu, X.; et al. Confinement and synergy effect of bimetallic Pt-Mn nanoparticles encapsulated in ZSM-5 zeolite with superior performance for acetone catalytic oxidation. *Appl. Catal. B Environ.* **2022**, *309*, 121224. [[CrossRef](#)]
17. Tao, J.; Liu, Y.; Deng, J.; Jing, L.; Hou, Z.; Wei, L.; Wang, Z.; Dai, H. Methane Combustion over Zeolite-Supported Palladium-Based Catalysts. *Catalysts* **2023**, *13*, 1251. [[CrossRef](#)]
18. Gan, T.; Chu, X.; Qi, H.; Zhang, W.; Zou, Y.; Yan, W.; Liu, G. Pt/Al₂O₃ with ultralow Pt-loading catalyze toluene oxidation: Promotional synergistic effect of Pt nanoparticles and Al₂O₃ support. *Appl. Catal. B Environ.* **2019**, *257*, 117943. [[CrossRef](#)]
19. Peng, R.; Li, S.; Sun, X.; Ren, Q.; Chen, L.; Fu, M.; Wu, J.; Ye, D. Size effect of Pt nanoparticles on the catalytic oxidation of toluene over Pt/CeO₂ catalysts. *Appl. Catal. B Environ.* **2018**, *220*, 462–470. [[CrossRef](#)]
20. Asal, Y.M.; Al-Akraa, I.M.; Mohammad, A.M.; El-Deab, M.S. A competent simultaneously co-electrodeposited Pt-MnOx nanocatalyst for enhanced formic acid electro-oxidation. *J. Taiwan Inst. Chem. Eng.* **2019**, *96*, 169–175. [[CrossRef](#)]
21. Guo, P.; Zhan, Y.; Yang, Y.; Lu, T. Preparation of COFs Supported Pd as an Efficient Catalyst for the Hydrogenation of Aromatic Nitro. *Catal. Lett.* **2022**, *152*, 3725–3732. [[CrossRef](#)]
22. Zheng, Y.; Zhou, J.; Ma, Z.; Weng, X.; Cheng, L.; Tang, G. Preparation of a High-Silicon ZSM-5 Molecular Sieve Using Only Coal Gangue as the Silicon and Aluminum Sources. *Materials* **2023**, *16*, 4338. [[CrossRef](#)] [[PubMed](#)]
23. Fu, Y.; Guo, D.; Jiang, W.; Tao, S.; Wang, X.; Yu, S.; Song, Z.; Liu, Y. Rapid synthesis of hierarchical silicoaluminophosphate molecular sieves using carbon-silicon composites from rice husk ash for deoxygenation of stearic acids. *Fuel* **2023**, *335*, 126956. [[CrossRef](#)]
24. Ren, S.; Yang, F.; Tian, C.; Yue, Y.; Zou, W.; Hua, W.; Gao, Z. Selective Alkylation of Benzene with Methanol to Toluene and Xylene over H-ZSM-5 Zeolites: Impact of Framework Al Spatial Distribution. *Catalysts* **2023**, *13*, 1295. [[CrossRef](#)]
25. Kalvachev, Y.; Todorova, T.; Kolev, H.; Merker, D.; Popov, C. Benzene Oxidation over Pt Loaded on Fly Ash Zeolite X. *Catalysts* **2023**, *13*, 1128. [[CrossRef](#)]
26. Hanaoka, T.; Aoyagi, M.; Edashige, Y. Improvement of n-Butene Yield in Dimethyl Ether-to-Olefin Reaction Using Ferrierite Zeolite Catalysts. *Catalysts* **2023**, *13*, 1040. [[CrossRef](#)]
27. Maharani, D.K.; Sanjaya, I.G.M.; Amaria, A.; Anggraeni, M.A.; Jannah, L.R. Molecular Docking Analysis Chitosan-Zeolite-ZnO Nanocomposite and Its Potency Against SARS-CoV-2. *IOP Conf. Ser. Mater. Sci. Eng.* **2021**, *1125*, 012006. [[CrossRef](#)]
28. Song, J.; Huang, Z.-F.; Pan, L.; Li, K.; Zhang, X.; Wang, L.; Zou, J.-J. Review on selective hydrogenation of nitroarene by catalytic, photocatalytic and electrocatalytic reactions. *Appl. Catal. B Environ.* **2018**, *227*, 386–408. [[CrossRef](#)]
29. Downing, R.S.; Kunkeler, P.J.; van Bekkum, H. Catalytic syntheses of aromatic amines. *Catal. Today* **1997**, *37*, 121–136. [[CrossRef](#)]
30. Liu, H.; Deng, Z.; Wang, B.; Ding, Z.; Li, Z. Efficient visible light-initiated hydrogenation of nitrobenzene for chemoselective production of aniline, azoxybenzene, azobenzene and hydrazobenzene over CQDs/CdS nanocomposites. *Dalton Trans.* **2023**, *52*, 13129–13136. [[CrossRef](#)]
31. Tong, F.; Liang, X.; Ma, F.; Bao, X.; Wang, Z.; Liu, Y.; Wang, P.; Cheng, H.; Dai, Y.; Huang, B.; et al. Plasmon-Mediated Nitrobenzene Hydrogenation with Formate as the Hydrogen Donor Studied at a Single-Particle Level. *Acs Catal.* **2021**, *11*, 3801–3809. [[CrossRef](#)]
32. Wang, L.; Yang, D.; Alhumade, H.; Yi, H.; Qi, X.; Lei, A. Revealing the Solution Structure of Pd(OAc)₂ with Halide Additives. *Chin. J. Chem.* **2022**, *40*, 895–901. [[CrossRef](#)]
33. Zhao, S.; Li, H.; Zhang, W.; Wang, B.; Yang, X.; Peng, Y.; Zhang, Y.; Li, Z. Insight into Crystallization Features of MOR Zeolite Synthesized via Ice-Templating Method. *Catalysts* **2022**, *12*, 301. [[CrossRef](#)]
34. Wang, J.; Li, M.; Fu, Y.; Amoo, C.C.; Jiang, Y.; Yang, R.; Sun, X.; Xing, C.; Maturura, E. An ambient pressure method for synthesizing NaY zeolite. *Microporous Mesoporous Mater.* **2021**, *320*, 111073. [[CrossRef](#)]
35. Santos, B.P.; Almeida, D.D.; Marques, M.D.F.V.; Henriques, C.A. Degradation of Polypropylene and Polyethylene Wastes Over HZSM-5 and USY Zeolites. *Catal. Lett.* **2019**, *149*, 798–812. [[CrossRef](#)]
36. Duan, Y.; Zhang, C.; Deng, D.; Sui, D.; Gao, X.; Yang, Y. Hydrogenation of BHMF with controllable selectivity to tetrahydropyranone and 1-hydroxy-2,5-hexanedione under atmospheric H₂ pressure. *Green Chem.* **2023**, *25*, 1823–1834. [[CrossRef](#)]

37. Khder, A.S.; Altass, H.M.; Jassas, R.S.; Al-Rooqi, M.M.; Khder, M.A.; Morad, M.; Gebreil, A.; Moussa, Z.; Ahmed, S.A. Room-Temperature CO Oxidation over Au-Pd Monometallic and Bimetallic Nanoparticle-Supported MgO. *Acs Appl. Nano Mater.* **2023**, *6*, 4243–4252. [[CrossRef](#)]
38. Yin, D.; Zhang, J.; Li, W.; Fu, Y. Hyaluronic Acid-Guided Synthesis of Pd Nanocatalysts for Transfer Hydrogenation of 4-Nitrophenol. *Catal. Lett.* **2021**, *151*, 1902–1910. [[CrossRef](#)]
39. Duan, Y.; Zheng, M.; Li, D.; Deng, D.; Wu, C.; Yang, Y. Synthesis of Pd/SBA-15 catalyst employing surface-bonded vinyl as a reductant and its application in the hydrogenation of nitroarenes. *RSC Adv.* **2017**, *7*, 3443–3449. [[CrossRef](#)]
40. Duan, Y.; Zheng, M.; Li, D.; Deng, D.; Ma, L.F.; Yang, Y. Conversion of HMF to methyl cyclopentenolone using Pd/Nb₂O₅ and Ca–Al catalysts via a two-step procedure. *Green Chem.* **2017**, *19*, 5103–5113. [[CrossRef](#)]
41. Tang, Q.; Yuan, Z.; Jin, S.; Yao, K.; Yang, H.; Chi, Q.; Liu, B. Biomass-derived carbon-supported Ni catalyst: An effective heterogeneous non-noble metal catalyst for the hydrogenation of nitro compounds. *React. Chem. Eng.* **2020**, *5*, 58–65. [[CrossRef](#)]
42. Fronczak, M.; Kasprzak, A.; Bystrzejewski, M. Carbon-encapsulated iron nanoparticles with deposited Pd: A high-performance catalyst for hydrogenation of nitro compounds. *J. Environ. Chem. Eng.* **2021**, *9*, 104673. [[CrossRef](#)]
43. Patra, A.K.; Vo, N.T.; Kim, D. Highly robust magnetically recoverable Ag/Fe₂O₃ nanocatalyst for chemoselective hydrogenation of nitroarenes in water. *Appl. Catal. A Gen.* **2017**, *538*, 148–156. [[CrossRef](#)]
44. Li, J.; Zhang, L.; Liu, X.; Shang, N.; Gao, S.; Feng, C.; Wang, C.; Wang, Z. Pd nanoparticles supported on a covalent triazine-based framework material: An efficient and highly chemoselective catalyst for the reduction of nitroarenes. *New J. Chem.* **2018**, *42*, 9684–9689. [[CrossRef](#)]
45. Li, Y.; Liu, H.; Ma, L.; He, D. Synergistic effect between Pd and Re on Pd-Re/SBA-15 catalysts and their catalytic behavior in glycerol hydrogenolysis. *Rsc Adv.* **2016**, *6*, 38680–38689. [[CrossRef](#)]
46. Howeizi, J.; Taghvaei-Ganjali, S.; Malekzadeh, M.; Motiee, F.; Sahebdehfar, S. Effect of the distribution and dispersion of palladium nanoparticles on the reducibility and performance of Pd/Al₂O₃ catalyst in liquid-phase hydrogenation of olefins. *React. Kinet. Mech. Catal.* **2020**, *130*, 777–795. [[CrossRef](#)]
47. Chen, H.; Zhang, R.; Wang, H.; Bao, W.; Wei, Y. Encapsulating uniform Pd nanoparticles in TS-1 zeolite as efficient catalyst for catalytic abatement of indoor formaldehyde at room temperature. *Appl. Catal. B Environ.* **2020**, *278*, 119311. [[CrossRef](#)]
48. Prekob, Á.; Muránszky, G.; Kocserha, I.; Fiser, B.; Kristály, F.; Halasi, G.; Kónya, Z.; Viskolcz, B.; Vanyorek, L. Sonochemical Deposition of Palladium Nanoparticles onto the Surface of N-Doped Carbon Nanotubes: A Simplified One-Step Catalyst Production Method. *Catal. Lett.* **2020**, *150*, 505–513. [[CrossRef](#)]

Disclaimer/Publisher’s Note: The statements, opinions and data contained in all publications are solely those of the individual author(s) and contributor(s) and not of MDPI and/or the editor(s). MDPI and/or the editor(s) disclaim responsibility for any injury to people or property resulting from any ideas, methods, instructions or products referred to in the content.